PAPER

Check for updates

Enhanced biocidal activity of Pr^{3+} doped yttrium silicates by Tm^{3+} and Yb^{3+} co-doping†

Patryk Fałat, [a] Min Ying Tsang,[ab] Irena Maliszewska, [c] Szymon J. Zelewski, [d] Bartłomiej Cichy, [e] Tymish Y. Ohulchanskyy, [f] Marek Samoć,[a] Marcin Nyk [a] and Dominika Wawrzyńczyk [*a]

We present an enhancement of optically triggered anti-microbial treatment based on visible to ultraviolet up-conversion emission in lanthanide-doped yttrium silicates. A series of Pr^{3+}/Tm^{3+}/Yb^{3+} co-doped Y$_2$Si$_2$O$_7$ powders was synthesized and characterized, including determination of their crystal structure, morphology, and spectroscopic properties. The emphasis was put on the examination of the influence of lanthanide ion doping on the luminescence characteristics in the ultraviolet region of light, since the emission from this part of the spectra can be effectively used for decontamination purposes. Due to the additional Tm^{3+} doping into the Pr^{3+} containing Y$_2$Si$_2$O$_7$ powders, we observed up-conversion emission lines in both UVA and UVC regions of spectra, while the solely Pr^{3+} doped materials gave only the emission in the UVC region. The synthesized luminescent powders were further used for decontamination experiments with three different types of pathogenic microorganisms (*i.e.*, *A. baumannii*, *S. aureus*, and *C. albicans*) formed biofilms. The microbial cell viability studies demonstrated the higher deactivation efficiency for all investigated microbial species with the use of combined UVA and UVC irradiation generated by Pr^{3+} and Tm^{3+} co-doped phosphors. At the same time, the incorporation of Yb^{3+} ions could additionally offer an alternative NIR-to-UVA excitation pathway *via* a 980 nm laser diode, which is beneficial for deeper light penetration experiments.

Introduction

The growing requirements of quality and health standards in, just to name a few, food processing, agriculture, healthcare, households, cosmetics, and pharmaceutics demand increasing use of disinfectants. This in turn results in the emergence of resistant cells[1] and resistant populations through vertical and

horizontal gene transfer,[2] and thus the so-called cross-resistance (correlation between resistance to antibiotics and disinfectants in bacteria) is becoming a concern of medical issue.[3] As early as in 2001 the World Health Organization (WHO) emphasized the importance of this problem, by publishing a document pointing out the need to limit the use of common antimicrobials to slow down the emergence of highly resistant strains (WHO Global Strategy for Containment of Antimicrobial Resistance).[4] This widespread problem reinforces the need to look for other procedures to control microbial growth, with one very promising alternative being the biocidal capability of light. Ultraviolet (UV) radiation is known to be an effective solution for germicidal and disinfection applications, however, the impact of light from different UV regions, *i.e.*, UVA: 320–400 nm, UVB: 280–320 nm, and UVC: 200–280 nm, on bacterial or viral inactivation is significantly different.[5] The UVC light is found to be the most efficient radiation for direct DNA damage of microorganisms since the spatially localized therapeutic effect is attainable due to double-stranded DNA UVC radiation absorption, resulting in hydrogen bond breakage between nucleobases, followed by bond formation between neighboring pairs of thymine and cytosine.[6] Consequently, DNA replication inhibition leads to death of irradiated microorganisms.[7] On the other hand, the UVA light

^{a} *Institute of Advanced Materials, Faculty of Chemistry, Wroclaw University of Science and Technology, Wyb. Wyspianskiego 27, 50-370 Wroclaw, Poland. E-mail: dominika.wawrzynczyk@pwr.edu.pl*

^{b} *Institute of Functional Materials and Catalysis, Faculty of Chemistry, University of Vienna, Währinger Straße 42, A-1090 Wien, Austria*

^{c} *Department of Organic and Medicinal Chemistry, Faculty of Chemistry, Wroclaw University of Science and Technology, Wyb. Wyspianskiego 27, 50-370 Wroclaw, Poland*

^{d} *Department of Experimental Physics, Faculty of Fundamental Problems of Technology, Wroclaw University of Science and Technology, Wyb. Wyspianskiego 27, 50-370 Wroclaw, Poland*

^{e} *Institute of Low Temperature and Structure Research, Polish Academy of Sciences, Okolna 2, 50-422 Wroclaw, Poland*

^{f} *College of Physics and Optoelectronic Engineering, Shenzhen University, Nanhai Avenue 3688, Nanshan District, Shenzhen 518060, Guangdong, China*

† Electronic supplementary information (ESI) available: Schematic representation of luminescence processes, synthesis details, calculated cell parameters, spectroscopic studies, and bacterial inactivation studies. See DOI: https://doi.org/10.1039/d3ma00451a

can deactivate bacteria *via* pathogen damage and/or generation of reactive oxygen species (ROS).[8–10] Therefore, the possibility to engineer and generate specific UV emission lines in combination is essential to enhance bacterial or viral inactivation with the use of light,[11–14] the application of which is nowadays of great concern for human health. Up to now, the most common way to generate UV light is by dedicated lamps or light-emitting diodes, however, such applications are greatly limited mainly due to the lack of site specificity.[15,16] Another possible option for efficient UV emission generation is taking advantage of luminescent materials, especially lanthanide-doped phosphors. In those materials, two- or multi-photon sequential absorption processes, which occur between ladder-like energy levels,[17,18] provide the possibility to up-convert visible (Vis) and/or near infrared (NIR) light to radiation in a specific region (including UV, Vis or NIR light) opening the perspectives for efficient light triggered therapy and diagnostics.[19–21] It was also recently shown that the Vis-to-UVC up-conversion (UC) emission generation by Pr^{3+} doped $NaYF_4$ microparticles could occur even under sunlight, which opens wide perspectives for applications of UVC emitting nano- and micro-particles for construction of, *e.g.*, self-disinfection fabrics or surfaces.[22] Additionally, we have very recently proved that it is possible to observe a DNA denaturation effect upon Vis excitation of Pr^{3+}/Yb^{3+} co-doped $NaYF_4$ and $LiYF_4$ nanoparticles, by efficient Vis-to-UVC UC emission generation.[6] Similar studies were performed also for other types of lanthanide containing matrices (*e.g.*, YBO_3 or Ca_2SiO_4),[23,24] including UV light emission from Gd^{3+}, Tm^{3+} or Pr^{3+} doped materials,[25] with particularly promising results obtained from yttrium silicate (Y_2SiO_5 and $Y_2Si_2O_7$) phosphors, establishing those materials as being among the most efficient for Vis-to-UVC UC emission generation.[26,27] The Vis-to-UVC UC is of particular interest, since it does not require multiple (>2) photon sequential absorption to observe UVC emission (as in the case of NIR-to-UV UC), which increases the overall process efficiency.

Taking advantage of selected lanthanide doping, in order to further enhance the proven germicidal performance of yttrium silicate powders, in this work we introduce a new function of the $Y_2Si_2O_7$ material by tri-doping with Pr^{3+}, Tm^{3+}, and Yb^{3+} ions. Tm^{3+} ion incorporation results in an additional UVA emission band at *ca.* 370 nm upon Vis excitation, through the energy transfer between Pr^{3+} and Tm^{3+} ions. This in fact can considerably enhance the photoinactivation process of different microbial species, as the emission from the UVA region can activate ROS generation and complement the DNA degradation effect provided by the UVC emission.[10] Simultaneously, co-doping with Yb^{3+} for sensitization with lower energy radiation (*i.e.*, ~980 nm) leads to transfer between Yb^{3+} and Tm^{3+} ions and, consequently, results in NIR-to-UV UC emission, which could be beneficial when the exciting light propagates in a scattering medium. Fig. S1 (ESI†) summarizes the schematic energy level diagram with possible transitions that can be observed in the studied materials. For a proof-of-concept, the combined effect of different Vis-to-UV UC emissions generated by the studied lanthanide doped powders under 447 nm (and

980 nm) laser irradiation on three biofilm forming microorganisms (*i.e.*, *A. baumannii*, *S. aureus*, and *C. albicans*) was investigated. The obtained results clearly revealed the enhanced anti-microbial action of combined (UVC + UVA) emissions from Pr^{3+} and Tm^{3+} doped silicates, which can provide guidance for the design of novel high performance UV emitting materials for disinfection purposes. The proposed approach could be utilized for perpetual light-triggered sterilization at healthcare facilities (*e.g.*, hospital rooms and operating theaters), which is crucial in the fight with multidrug resistant superbacteria – one of the challenges modern medicine is nowadays struggling with.[28] The proof-of-concept experiments have already been reported: regenerative, anti-viral coatings for various types of surfaces[29] demonstrate the enveloped virus deactivation. The 447 nm laser diode excitation was used for *S. aureus* bacterial solution inactivation with Pr^{3+} doped $SrSiO_3$ powders,[30] while Zhao *et al.* constructed antibacterial wound dressings based on Vis-to-UVC up-conversion in Pr^{3+} doped materials.[31] Thus, any improvement in the materials performance in this spectral region could quickly be reflected in the development in technological solutions.

Experimental

Lanthanide doped $Y_2Si_2O_7$ phosphor synthesis

A series of lanthanide-doped $Y_2Si_2O_7$ phosphors (*i.e.*, undoped $Y_2Si_2O_7$; $Y_2Si_2O_7{:}Pr^{3+}$ and $Y_2Si_2O_7{:}Pr^{3+},Tm^{3+},Yb^{3+}$) was synthesized in accordance with the sol–gel synthesis protocol reported by Cates *et al.*[26] with slight modifications. In general, the total amount of 4.43 mmol of corresponding RE_2O_3 (RE = Y, Pr, Tm, Yb) was dissolved in a $HNO_3 : H_2O$ mixture (1 : 1 v/v) in a three-neck round-bottom flask under reflux with nitrogen purging for 1 h (please see Table S1 for the exact amounts of chemicals used, ESI†). The excess of solvent was evaporated with a rotary evaporator and the obtained powder was washed several times with small portions of deionized water until the pH was set to 7. After overnight drying on a hot plate at 130 °C in air, the precursor powder was dissolved in 3.25 mL of EtOH and 1.02 mL of deionized water, followed by the addition of 0.98 mL of TEOS. The solution was slowly stirred and heated at 70 °C to form a clear gel, which was later dried in an oven in the air for 17 h at 104 °C. The obtained powders were ground in a mortar and placed into alumina crucibles, which were heated in a muffle furnace at a 8 °C min^{-1} rate for calcination under an ambient atmosphere for 3 h at 1000 °C. The calcined phosphors were cooled down naturally to room temperature.

Morphology and structure characterization

Powder X-ray diffraction (XRD) analysis of the obtained materials was performed on a Bragg–Brentano geometry STOE X-ray diffractometer using Cu Kα radiation. The 2θ range was 10–80°. The crystal phases (and cell parameters) of the synthesized powders were determined based on the Rietveld refinement procedure. Scanning electron microscopy (SEM) images were captured with a Jeol JSM-6610LVnx scanning electron

microscope (accelerating voltage: 10–15 kV, WD: 10 mm). Elemental analysis was conducted with an integrated Oxford Aztec Energy X-ray energy-dispersive spectrometer working together with the same Jeol SEM microscope.

Optical spectroscopy

All of the spectroscopic studies were conducted at room temperature in ambient air for powder samples. As the main purpose of the presented study was to show the effect of Tm^{3+} co-doping on the emission in the UV region and thus the efficiency of studied materials in bacteria deactivation, the obtained spectroscopic results should be treated in a qualitative manner. The down-conversion (DC) emission and luminescence lifetimes in the Vis spectral range were obtained upon 447 nm excitation using a FLS980 Edinburgh Instruments photoluminescence spectrometer. The Vis-to-UVC UC and NIR-to-UV UC was measured using the experimental setup described in our previous work.[6] In short, the emission from lanthanide-doped phosphors was induced with either a focused 447 nm fiber-coupled semiconductor laser diode (CNI Laser), or a 980 nm fiber-coupled semiconductor laser diode (CNI Laser), modulated with a mechanical chopper. In the case of Vis-to-UVC measurements the emitted radiation passed through an optical setup constructed of UV silica lenses and a set of filters to cut off the scattered laser light. The spectra were analyzed with a grating monochromator (Horiba iHR320) coupled with a pre-amplified photomultiplier tube (PMT, Hamamatsu H5784-04), with the PMT signal demodulated with a lock-in amplifier (EG & G 7260). Vis-to-UV UC luminescence lifetime measurements were obtained with the same experimental setup, with the 447 nm laser directly modulated with a square wave generated by the lock-in amplifier. The PMT signal was passed through a 200 MHz high input impedance voltage amplifier (Femto HVA-200M-40-F) to ensure a high dynamic range and measured with a digital oscilloscope (Rohde & Schwarz RTB2K, 300 MHz bandwidth).

Biocidal studies

MTT reagent (Sigma Aldrich, Poland) was prepared by dissolving 3-(4,5-dimethylthiazol-2-yl)-2,5-diphenyltetrazolium bromide in phosphate buffer saline (PBS) (pH = 7.2) to a final concentration of 5 g L^{-1}; the solution was stored at 4 °C. Acidic isopropanol was prepared using 50 mL of isopropanol and 0.75 mL of HCl. For photo-induced inactivation studies the CW laser diode (non-focused) with the peak-power wavelength at 447 nm and 980 nm (CNI Laser) at the output power density of $\sim$800 mW cm^{-2}, and $\sim$500 mW cm^{-2} were used, respectively. Additionally, the control experiment by using a UV emitting lamp (a wavelength of 254 nm; 2-wavelength UV lamp Kamus LP254UV) for photo-induced inactivation studies in the absence of powders was performed. Three microbial species were used in this study: *Acinetobacter baumannii* (PCM 8740), *Staphylococcus aureus* (PCM 2024) and *Candida albicans* (ATCC 10231). One colony of each test organism was inoculated in 5 mL of Mueller–Hinton Broth (Oxoid). In the case of *C. albicans*, this medium was supplemented with 1% glucose.

The suspensions were incubated for 24 h in the dark at 37 °C. After this time, each culture was centrifuged separately (5 min/6000 rpm) and the obtained pellet was suspended in 5 mL of sterile PBS to give an inoculum of approximately 1–2 × 10^6 colony-forming units (CFU mL^{-1}).

Biofilm formation

At first, 100 μL of a standardized cell suspension of *A. baumannii*, *S. aureus* and *C. albicans* was transferred into each well of a pre-sterilized polystyrene flat-bottom 96 well plate and incubated for 4 h in the dark. After this time, the supernatant (containing non-adhered cells) was removed from each well and the plates were washed using 100 μL of sterile PBS. Then, 100 μL of fresh Mueller-Hinton Broth (in the case of *C. albicans* the medium was supplemented with 1% glucose) was added to each well and the plates were further incubated for 24 h in the dark at 37 °C for biofilm development. Next, the supernatant was removed again and the wells were washed with 100 μL of sterile PBS.

Dark cytotoxicity studies

Studies on the biocidal effectiveness of powder materials were preceded by the determination of dark cytotoxicity. The dark cytotoxicity of $Y_2Si_2O_7$, $Y_2Si_2O_7$:Pr^{3+} and $Y_2Si_2O_7$:Pr^{3+},Tm^{3+},Yb^3 was determined against planktonic and biofilm cultures (see the ESI†). Briefly, 5, 15 or 30 mg of the tested powder materials were added to each well of a 96 well flat-bottom microtiter plate (Thermo Scientific™) containing planktonic or biofilm cultures of *A. baumannii*, *S. aureus*, *B. cereus*, and *C. albicans*. The plate was then incubated at 37 °C, without shaking and for 24 h (in the dark). The cell viability after 1, 4, and 8 h was determined using a BacTiter-Glo™ test (planktonic culture) (see the ESI†) or MTT test (biofilm culture) using the previously described protocol.[32] The cultures of the studied microorganisms were incubated under the same reaction conditions and were used as controls. The study was carried out in triplicate.

Biocidal effect studies

Based on the determined dark cytotoxicity (see the ESI†), powder materials at a concentration of 30 mg per well were used in all biofilm disruption experiments. All experiments were preceded by examining the effect of light irradiation alone on the viability of biofilm formed by *A. baumannii*, *S. aureus*, and *C. albicans*. These studies were carried out by irradiating the biofilms with laser light for 5, 7 and 10 minutes, and cell viability was assessed using an MTT test using the previously described protocol.[32] The non-toxic light dose has been defined as the exposition time causing a decrease in cell viability by no more than 20%. To study the effect of $Y_2Si_2O_7$, $Y_2Si_2O_7$:Pr^{3+} and $Y_2Si_2O_7$:Pr^{3+},Tm^{3+},Yb^{3+} on the inactivation of biofilms, 30 mg of the tested powder materials were added to each well (with formed biofilm), and then the microorganisms were irradiated with laser light for 10 min. The viability of the cells was determined by the MTT assay. The study was carried out in duplicate.

The reduction in microbial biofilm viability was calculated using the following formula:

$$\frac{(AI - AB) - (AT - AB) \times 100\%}{AI - AB}$$

where:

AI-absorbance of the initial sample (biofilm before photo-inactivation)

AB-absorbance of the background sample (no cells, 0.015)

AT-absorbance of the tested sample (biofilm after photo-inactivation).

Studies on the generation of intracellular reactive oxygen species

Following 447 nm irradiation in the presence of $Y_2Si_2O_7$, $Y_2Si_2O_7$:Pr^{3+}, and $Y_2Si_2O_7$:Pr^{3+},Tm^{3+},Yb^{3+} powders, biofilm formed by *S. aureus*, was incubated with a solution of 2′,7′-dichlorodihydrofluorescein diacetate (DCFDA) at a final concentration of 50 μM. Next, the generation of ROS was detected with the spectrofluorimetric method with excitation at 485 nm and emission at 520 nm using a SpectraMax Gemini spectrofluorimeter and the SoftMaxPro5 software.

Statistical analysis

The statistical analysis was performed using the STATISTICA data analysis software (version 10.0) and Microsoft Excel. The quantitative variables were characterized by the arithmetic mean of standard deviation or median or max/min (range) and 95% confidence interval. The statistical significance of the differences between two groups was processed with the Student's *t* test. In all the calculations, the *p* value of 0.05 was used as the limit value.

Results and discussion

Morphology and crystal structure

A series of lanthanide-doped (*i.e.*, Pr^{3+}, Yb^{3+}, Tm^{3+}) $Y_2Si_2O_7$ polycrystalline powder materials was synthesized, and the corresponding SEM images of the obtained powders are presented in Fig. 1. The undoped (Fig. 1a) and solely Pr^{3+} doped (Fig. 1b) materials showed highly fused crystallites, while further co-doping with Tm^{3+} and Yb^{3+} ions resulted in smaller crystallite formation (Fig. 1c). The EDS images complementary to the morphology characterization confirmed the homogeneous distribution of doping ions within the samples (Fig. 1b and c). The observed changes in morphology upon high doping were further confirmed by the XRD results. X-ray diffraction data (Fig. 1) and Rietveld refinement based analysis (Table S2, ESI†) revealed that Pr^{3+}, Tm^{3+}, and Yb^{3+} incorporation into the host matrix does influence the crystal structure. Based on the Rietveld refinement, all the materials were assigned to the $Y_2Si_2O_7$ structure (Fig. 1 shows the measured XRD patterns together with the calculated ones and assignment of major intensity peaks with the colored asterisks), although the peak position and intensities do not coincide exactly with the standard patterns. The undoped (Fig. 1a) and solely Pr^{3+} doped (Fig. 1b) materials showed a dominant triclinic phase ($P\bar{1}$) in the XRD spectra of $\sim$75% and $\sim$90% amount, respectively. The main reflections in the measured XRD spectra matched the mp-581644 card (Fig. 1a and 1b). Further co-coping with Tm^{3+} and Yb^{3+} ions resulted in a phase change to the pure triclinic ($P\bar{1}$) one (Fig. 1c). The higher phase purity for the oxide-based powder phosphorus in response to additional doping (*e.g.*, Li^+ or Lu^{3+}) was in fact reported previously.[26,33,34] The main mechanism postulated for this phenomena is related to the flux effect (formation of the liquid phase at the grain boundaries), which can enhance the rate of crystallite formation, leading to the formation of crystallites of higher crystal structure purity during the annealing process.[35] The calculated cell parameters (Table S2, ESI†) show some divergence from the average values observed in silicates, but are comparable to those observed in other related disilicates, *e.g.*, $Ho_2Si_2O_7$ or $Dy_2Si_2O_7$.[36,37] The crystal structure of $Y_2Si_2O_7$ belongs to the group of so-called mixed anion silicates,[38] a polymorphs material with low symmetry where every atom has a separately defined site in this type of structure, thus any doping can lead to changes in the XRD reflex position or relative intensity. The Y^{3+}, Pr^{3+}, Yb^{3+} and Tm^{3+} differ in X-ray scattering factors, thus influence the intensity and position of the observed XRD lines. Additionally, the miscibility of doping ions in the Y site can have an impact on the final XRD spectra.[34] The Rietveld refinement was in our case performed for ideal structure models that did not match fully the real structures, thus it was tricky and challenging to obtain a perfect match between the measured and theoretical XRD patterns. However, based on the obtained Rietveld refinement, still closely matching the model structures, we can still confirm the validity of the crystal phase of the obtained materials.

Photoluminescence spectroscopy

As the structures of all synthesized samples were confirmed as a $Y_2Si_2O_7$ polymorph, further spectroscopic analyses were conducted to investigate the energy transfer between the lanthanides and the possibility of manipulating the UV emission output. The DC emission of $Y_2Si_2O_7$:Pr^{3+} excited by the 447 nm laser was peaked at *ca.* 490 nm, 540 nm, 610 nm, 650 nm, 710 nm, and 735 nm (Fig. 2a), which corresponds to the $^3P_0 \rightarrow \,^3H_4$, $^3P_0 \rightarrow \,^3H_5$, $^3P_0 \rightarrow \,^3H_6$, $^3P_0 \rightarrow \,^3F_2$, $^3P_0 \rightarrow \,^3F_3$, and $^3P_0 \rightarrow \,^3F_4$ electronic transitions within the Pr^{3+} ion energy levels, respectively (see Fig. S1a for the energy level scheme, ESI†).[39]

Further co-doping of Tm^{3+} resulted in the appearance of additional bands peaked at *ca.* 470 nm, 650 nm and 735 nm, which could be ascribed to $^1G_4 \rightarrow \,^3H_6$, $^1G_4 \rightarrow \,^3F_4$, and $^1G_4 \rightarrow \,^3H_5$ electronic transitions in the Tm^{3+}, respectively (see Fig. 2b for spectra and Fig. S1b for the energy diagram, ESI†), as incorporation of Tm^{3+} ions can be sensitized by energy transfer between the $^3P_0$ excited state of Pr^{3+} ions and $^1G_4$ energy level of Tm^{3+} ions.[40] The observed emission lines are similar to those reported for Pr^{3+} or Tm^{3+} doped yttrium silicates materials.[40,41] To confirm the energy transfer between Pr^{3+} and Tm^{3+} ions we have additionally measured the luminescence lifetime of Pr^{3+}
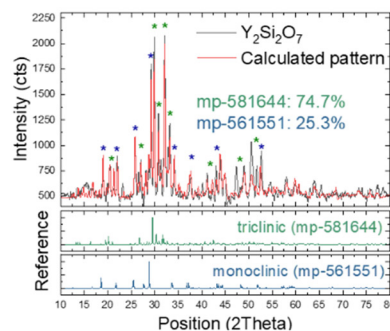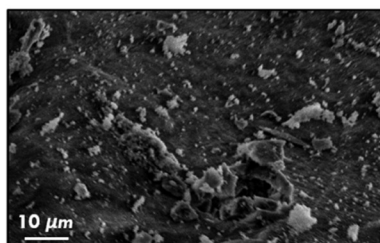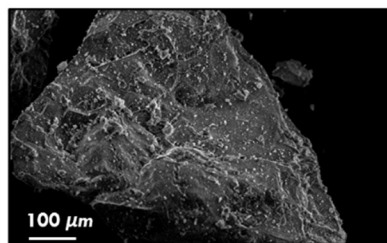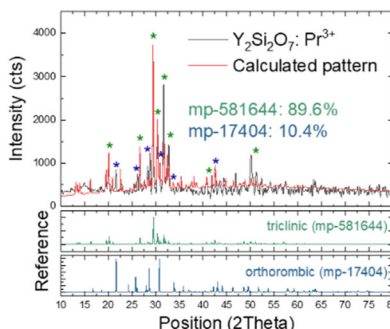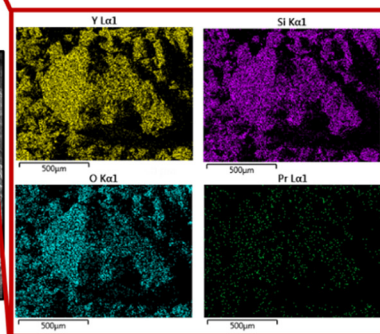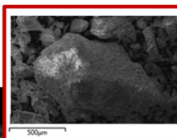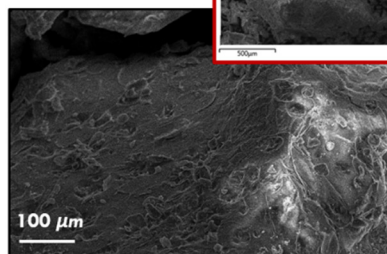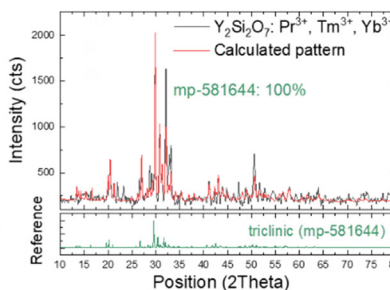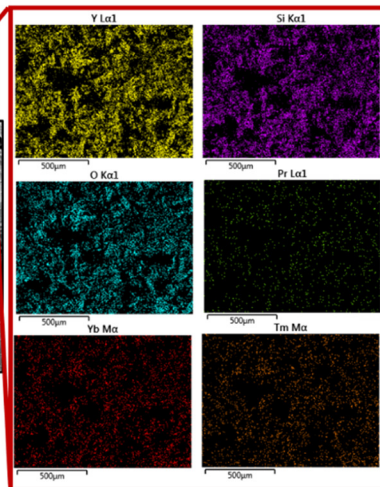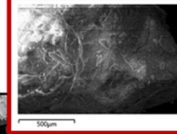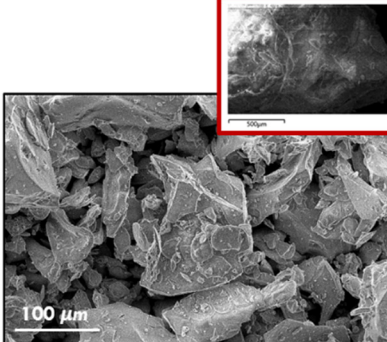
Fig. 1 Characterization of morphology – SEM images, composition – EDS maps and crystal structure – measured and calculated XRD patterns of un-doped $Y_2Si_2O_7$ (a), $Y_2Si_2O_7$:Pr^{3+} (b) and $Y_2Si_2O_7$:Pr^{3+},Tm^{3+},Yb^{3+} powders.

ions $^3P_0$ excited level by monitoring the decay curves at 610 nm (Fig. 2c). The studied samples showed a double-exponential decay behaviour, and a significant shortening of τ values, both short and long components, was observed for samples co-doped with Tm^{3+} ions. The former decreased from 46.22 µs down to 2.7 µs, while the latter from 122.2 µs down to 14.56 µs upon Tm^{3+} co-doping (Fig. 2c). The results of measurements of emission kinetics thus support the ones obtained in the steady-state, and confirm the efficient energy transfer between Pr^{3+} and Tm^{3+} ions. Moreover, upon 980 nm excitation of the $Y_2Si_2O_7$:Pr^{3+},Tm^{3+},Yb^{3+} sample emission peaks at *ca.* 480 nm, 650 nm, and 790 nm are observed, which correspond to the $^1G_4 \rightarrow {}^3H_6$, $^1G_4 \rightarrow {}^3F_4$, and $^3H_4 \rightarrow {}^3H_6$ electronic transitions in Tm^{3+} ions, respectively (Fig. S2, ESI†). This is because of the

energy transfer occurring only between Yb^{3+} and Tm^{3+} (see Fig. S1c for the energy level diagram, ESI†), in agreement with the reported up-conversion emission bands in Yb^{3+} and Tm^{3+} co-doped materials.[42,43]

Having acquired the Vis DC emission spectra and confirmed the corresponding energy transfer between Pr^{3+} and Tm^{3+} in the synthesized materials, we further investigated the UC emission in the UV region under Vis (447 nm, Fig. 3a and b) and NIR (980 nm, Fig. 3c) excitations. Upon 447 nm excitation, two broad bands ranging between ~250 nm to ~390 nm with maximum emission intensity at 278 nm and 308 nm are observed (Fig. 3a and b). This is the consequence of sequential absorption of two blue photons, as confirmed by the measure-ments of power dependence of UV emission (slopes of the
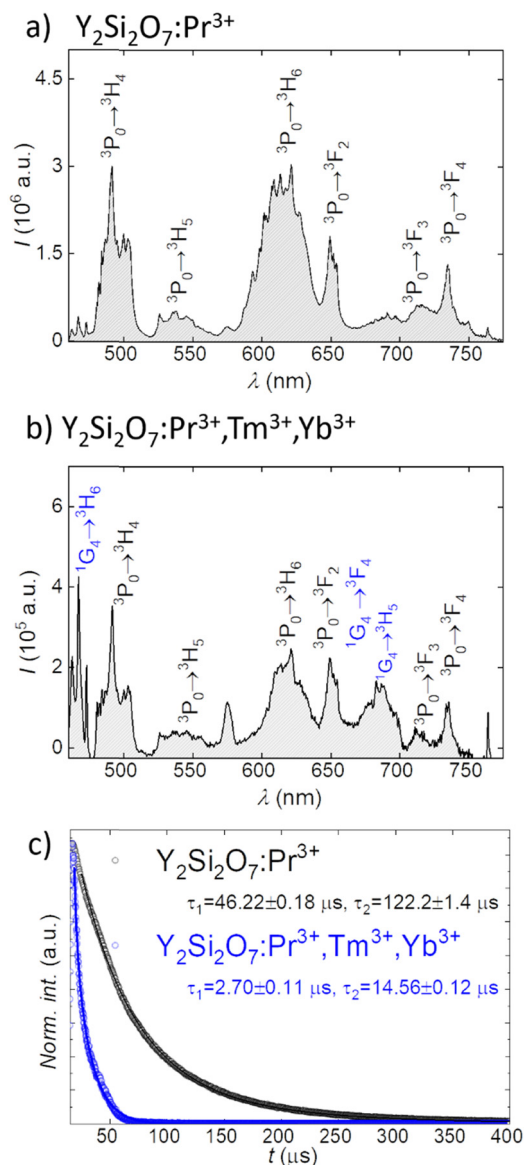
Fig. 2 Down-conversion emission spectra of $Y_2Si_2O_7:Pr^{3+}$ (a) and $Y_2Si_2O_7:Pr^{3+},Tm^{3+},Yb^{3+}$ (b) phosphors upon 447 nm excitation together with fluorescence decay curves recorded at 610 nm upon 447 nm excitation for Pr^{3+}-based $Y_2Si_2O_7$ silicates (c).

Fig. 3 Vis-to-UVC UC spectra of $Y_2Si_2O_7:Pr^{3+}$ (a) and $Y_2Si_2O_7:Pr^{3+},Tm^{3+},Yb^{3+}$ (b) powders upon 447 nm CW laser irradiation at a power of 1000 mW. The insets show log–log plots of integrated intensity vs. excitation power with the linear fits and slope values. NIR-to-UV UC spectrum of $Y_2Si_2O_7:Pr^{3+},Tm^{3+},Yb^{3+}$ (c) upon 980 nm CW laser irradiation at a power of 1000 mW.

log–log excitation power vs. emission intensity plots are equal to approximately 2 as presented in the insets in Fig. 3a and b). In this UC process first the $^3P_0$ energy level of Pr^{3+} ions is populated followed by the excited state absorption to the 4f5d energy level of the matrix, and finally the $4f5d \rightarrow {}^3H_4$ depopulation is observed giving rise to the UV emission, as presented schematically in Fig. S1d (ESI†) and consistent with the previously reported results.[6,44] Additionally, UC emission decay curves were acquired at 278 and 308 nm (Fig. S3, ESI†), and the experimentally obtained decay curves were fitted onoexponentially, showing luminescence lifetimes of 12.34 µs for emission at 278 nm and 8.86 µs for UV UC emission decay measured at 308 nm. When additional Tm^{3+} and Yb^{3+} ions are introduced,
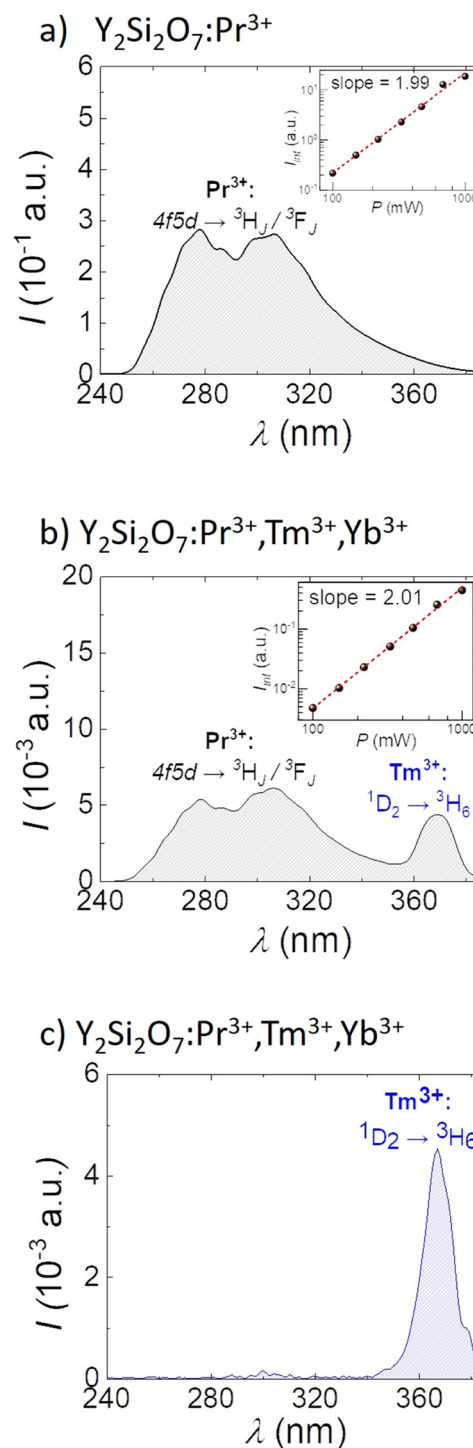
the UC emission spectra show an additional narrow band at ~370 nm (Fig. 3c), which corresponds to the $^1D_2 \rightarrow {}^3H_6$ f–f electronic transition of Tm^{3+} ion (see Fig. S1e for the energy

level diagram, ESI†). Its origin is ascribed to energy transfer from Pr^{3+} (which serves as a sensitizer upon 447 nm excitation) to Tm^{3+}. Upon 980 nm excitation, the NIR-to-UVA UC can also be achieved *via* multiple energy transfer between sensitized Yb^{3+} and activated Tm^{3+} (see Fig. S1c for the energy level diagram, ESI†). This can be clearly seen in Fig. 3c, as the emission band at *ca.* 370 nm appears, corresponding to the $^1D_2 \rightarrow {}^3H_6$ electronic transition in Tm^{3+} ions. Based on the presented spectroscopy results, one can suggest the application of co-doped $Y_2Si_2O_7$ materials for anti-microbial purposes, since all of the studied phosphors showed intense emission in the different UV regions when excited with Vis 447 nm or NIR 980 nm laser light. We also suggest a possible manifestation of an additional phototoxic effect from Tm^{3+} co-doped systems, since the PL emission peaked at *ca.* 370 nm is able to excite endogenous porphyrins within the bacteria, leading to the generation of ROS, such as hydroxyl radicals and hydrogen peroxide.[45,46]

Microbial inactivation studies

As a proof-of-concept for microbial inactivation application, we tested the biocidal effect with different Vis-to-UV UC emission (UVA and UVC) and NIR-to-UVA UC emission generated from $Y_2Si_2O_7$:Pr^{3+} and $Y_2Si_2O_7$:Pr^{3+},Tm^{3+},Yb^{3+} materials on biofilm

formed by *A. baumannii*, *S. aureus* and *C. albicans*. A schematic representation of the experiment is presented in Fig. 4a. Therefore, we could evaluate the influence of the additional UVA band generated by Tm^{3+} doping on the anti-microbial efficiency compared to the solely Pr^{3+} doped silicates. Biofilm, defined as a structured gathering of microbes adhering to each other and/or to a surface that is often embedded in a self-produced matrix of extracellular polymeric material, is commonly used for understanding the nature of microbial growth in different environments.[47] Additionally, it was indicated that biofilm bacteria are more resistant to antimicrobials than planktonic forms.[48] Low penetration of antibiotics/disinfectants into the biofilm, slow reproduction, and the existence of an adaptive stress response constitutes a multiphase defense of bacteria, making biofilm treatment difficult with effective doses of biocidal agents.[49,50] The phototoxic effect of lanthanide-doped $Y_2Si_2O_7$ powders on microbial cell viability after light treatment was evaluated using MTT assay.[51] This test provides a simple method for determining cell viability using the well-known and widely used reagent 3-(4,5-dimethylthiazol-2-yl)-2,5-diphenyltetrazolium bromide that is converted by nicotine adenine dinucleotide phosphate (NADPH)-dependent cellular oxidoreductase enzymes to insoluble formazan. Thus, the used assay determines cell viability in terms of reductive activity as
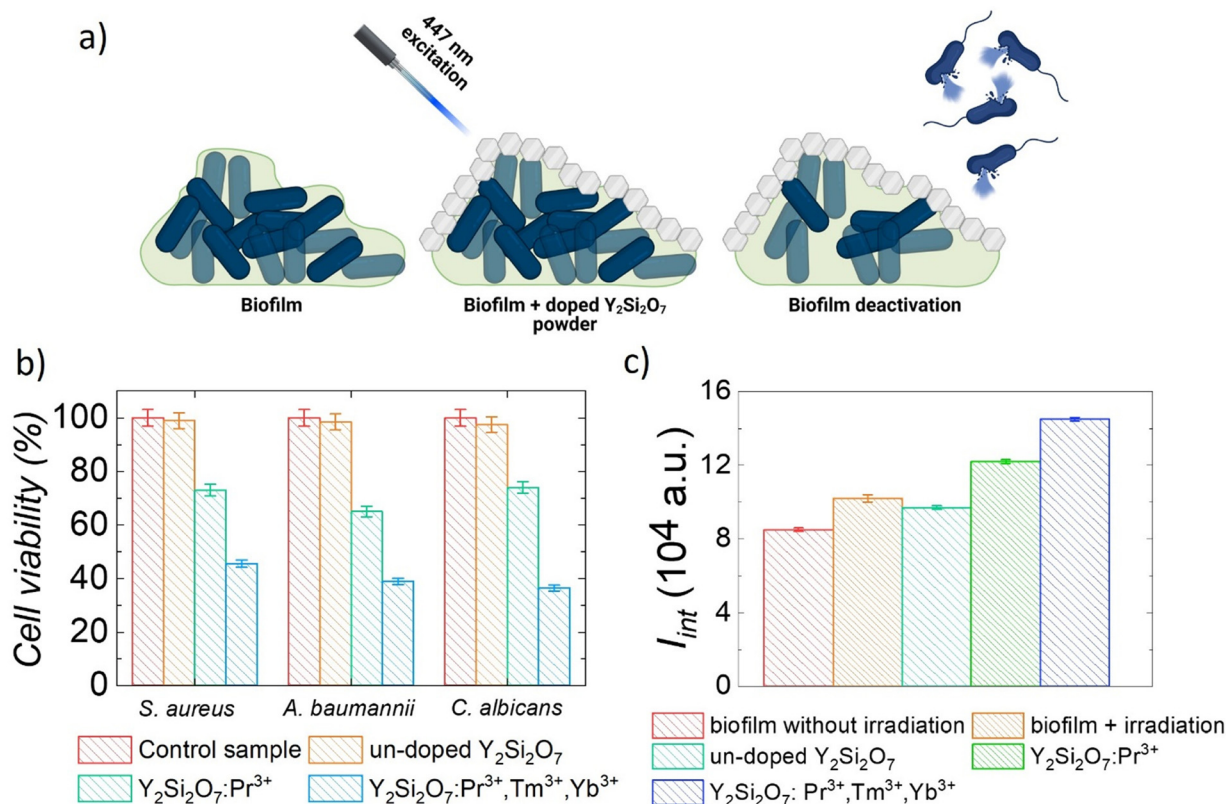

Fig. 4 (a): A schematic representation of the proof-of-concept experiment for using doped $Y_2Si_2O_7$ powders for biofilm deactivation purposes. (b): Viability of biofilm (*S. aureus*; *A. baumannii*, and *C. albicans*) cells after irradiation with 447 nm laser light (800 mW cm^{-2}) in the presence of un-doped $Y_2Si_2O_7$; $Y_2Si_2O_7$:Pr^{3+}, and $Y_2Si_2O_7$:Pr^{3+},Tm^{3+},Yb^{3+} and without them (control, 100% represents viability of non-irradiated cells). (c): Effectiveness of generating oxidative species in biofilm irradiated by a 447 nm laser diode (800 mW cm^{-2}) in the presence of un-doped $Y_2Si_2O_7$; $Y_2Si_2O_7$:Pr^{3+}; and $Y_2Si_2O_7$:Pr^{3+},Tm^{3+},Yb^{3+} phosphors.

an enzymatic conversion of a tetrazolium compound to formazan by dehydrogenases found in living cells. After solubilization of the formazan with the isopropanol, the concentration of the colorimetric probe was determined by optical density measurement at 570 nm. The photo-biocidal effect of laser light irradiation on biofilm formed by *S. aureus*, *A. baumannii*, and *C. albicans* was first determined. It was found that the 447 nm laser irradiation up to 10 min did not result in significant microbial cell death (mortality did not exceed $14 \pm 2\%$), therefore all subsequent biofilm photo-eradication experiments were carried out at a light dose of ~ 500 J cm^{-2}, which is equal to 10 min exposure of cells under laser light (447 nm, 800 mW cm^{-2}). The obtained results of photo-inactivation of biofilm formed by *S. aureus*, *A. baumannii*, and *C. albicans* at the presence of non-cytotoxic concentrations of the studied powder materials (ESI;† Table S3; 30 mg per well) are presented in Fig. 4b. The most significant reduction in viability of microbial cells after laser light treatment was observed in the presence of Y$_2$Si$_2$O$_7$:Pr^{3+},Tm^{3+},Yb^{3+} phosphors. When Y$_2$Si$_2$O$_7$:Pr^{3+},Tm^{3+},Yb^{3+} powder was used in the experiment as a source of UV light, the viability of biofilm-forming microorganisms depended on the species of pathogen and dropped down to $45.5 \pm 2.5\%$ (*S. aureus*), $39.0 \pm 3.0\%$ (*A. baumannii*) and $36.5 \pm 2.5\%$ (*C. albicans*). At the same time, the viability of cells treated with solely Pr^{3+} doped materials and irradiated in the same manner was also noticeably reduced (to ~ 65–75%), suggesting that a DNA damaging mechanism could also be involved. We expected that the lower cell viability with the use of Tm^{3+} co-doped yttrium silicates powders is due to the UVA light induced production of ROS that are toxic to living cells.[45,46] In order to validate this hypothesis, a fluorometric assay with dichlorodihydrofluorescein diacetate (DCFH-DA) was therefore carried out to detect oxidative stress in the bacteria cells under the influence of light activated un-doped Y$_2$Si$_2$O$_7$; Y$_2$Si$_2$O$_7$:Pr^{3+}, and Y$_2$Si$_2$O$_7$:Pr^{3+},Tm^{3+},Yb^{3+} phosphors (Fig. 4c).

As shown in Fig. 4c, after irradiating the biofilm for 10 min, the yield of generated ROS compounds increased, compared to the control sample (biofilm without irradiation), by $\sim 54 \pm 2\%$ in the presence of Y$_2$Si$_2$O$_7$:Pr^{3+} powders. This means that the mechanism of phototoxicity of the solely Pr^{3+} doped materials involves not only DNA damage, but also ROS generation. Moreover, the comparison of cell viability and ROS generation data suggests that this mechanism dominates at the given experimental conditions. The presence of Y$_2$Si$_2$O$_7$:Pr^{3+},Tm^{3+},Yb^{3+} resulted in more efficient generation of ROS ($70 \pm 2\%$), in comparison with the biofilm before irradiation. These findings clearly show that the higher efficiency of bacterial cell photo-killing in the presence of Y$_2$Si$_2$O$_7$:Pr^{3+},Tm^{3+},Yb^{3+} is the result of increased production of ROS. Finally, it is worth noting that very promising results on the destruction of both Gram-positive and Gram-negative planktonic bacteria and eukaryotic cells represented by *C. albicans* have been also obtained (the ESI† section on bacterial inactivation studies and Fig. S4). It has been shown that planktonic culture microbial cells can be effectively killed by the Vis-to-UV UC light generated from

lanthanide doped Y$_2$Si$_2$O$_7$ phosphors. Indeed, in some cases, the viability decreased even down to $\sim 2\%$, for example for planktonic cells of *A. baumannii* incubated with 30 mg per well of Y$_2$Si$_2$O$_7$:Pr^{3+},Tm^{3+},Yb^{3+} material and irradiated with a light dose of ~ 350 J cm^{-2} (Fig. S4a, ESI†). As expected, the efficiency of destroying planktonic cells was higher than that of the biofilm, since it is well known that cells in a biofilm are more resistant to destruction due to the presence of extracellular polymeric substances, highly hydrated polymers that are mainly composed of polysaccharides, proteins, and DNA, and protect cells from environmental stresses. The cell viability studies, which clearly demonstrated the higher deactivation efficiency of microbials under combined UVA and UVC irradiation from Y$_2$Si$_2$O$_7$:Pr^{3+},Tm^{3+},Yb^{3+} phosphors, have proven the effectiveness of the Vis-to-UVA and Vis-to-UVC UC process by co-doping Pr^{3+} and Tm^{3+} in the system. Our results are consistent with those previously reported by Karami *et al.*[52] who used NIR-activated-β-NaYF$_4$:Yb/Tm@ZnO nanoparticles (NPs) exhibiting significant antimicrobial activity against planktonic cultures of two strains of *S. aureus*. It has been estimated that the reduction in the number of viable cells was down to 78.8–82.6%. Tou *et al.*[53] synthesized core–shell–shell structures by sequentially coating SiO$_2$ and ZnO NPs on the surface of NaYF$_4$:Yb^{3+},Tm^{3+} ones, and showed that under the 980 nm excitation the studied material is capable for ROS generation leading to the biocidal effect. Those approaches, however, used 980 nm as excitation which is much more absorbed by water than 447 nm light used in the current study, and can lead to unwanted heating. Additionally, the NIR-to-UV UC process requires sequential absorption of more than two-photons to occur, and thus higher power excitation is needed, again leading to heat-related effects. Other authors showed significantly higher antimicrobial activity of studied materials, but it should be emphasized that in those approaches organic photosensitizers (PS) were applied, and the systems worked based on the energy transfer between lanthanide doped NPs and PS. Zhang *et al.*[54] showed an excellent antibacterial activity of NIR-activated LiYF$_4$:Yb^{3+},Er^{3+} NPs conjugated with zinc β-carboxyphthalocyanine and polyvinylpyrrolidone. The efficacy results showed 4.0–4.5 log$_{10}$ reductions in the viability of *E. coli* and 5 log$_{10}$ reductions in *S. aureus* (bactericidal activity was higher than 99.99%). Liu *et al.*,[55] studied the antimicrobial activity of LiYF$_4$:Yb^{3+},Er^{3+} NPs loaded with Rose Bengal as a PS, and it was found that these materials showed almost 100% antibacterial efficacy against drug-resistant *Acinetobacter baumannii*. Other types of NPs can also be considered for antimicrobial treatments, *i.e.*, it is known that among nanomaterials, silver (at low concentrations) is characterized by significant antimicrobial activity. Silver ions (Ag$^+$) released from the dissolution of metallic silver NPs are believed to be the basis for these antimicrobial effects.[56] However, attention should be paid to the rational use of silver as a biocide. Previously, it was shown that silver can be toxic to human cells.[57] Argyria is a serious disease that has been known for centuries, which is the result of frequent application of silver. Other known structures that have antimicrobial properties are Fe-doped,

ZnO, Nb/N-doped ZnO and Cu-doped TiO_2. It has already been shown that the mortality rate of suspension cultures of various microorganisms does not exceed 90%.

At the same time, the incorporation of Yb^{3+} ions can additionally offer an alternative NIR-to-UVA excitation pathway *via* a 980 nm laser diode, which could be beneficial for deeper light penetration. In fact we have performed a relevant experiment (Fig. S5, ESI†), however, we were forced to use low excitation powers since 980 nm light can lead to unwanted heating of water containing solutions (~ 500 mW cm^{-2}). As can be seen in the Fig. S5 (ESI†), the mortality rate of the tested pathogens did not exceed 6% (and fit within the limits of measurement error), thus showed that in this case the effect of 980 nm light with a dose of ~ 300 J cm^{-2}, which is equal to 10 min exposure of cells under laser light (980 nm, 500 mW cm^{-2}), on the viability of microorganisms was not observed. Additionally, as a control experiment we also checked the photo-inactivation of biofilm in which direct UV light irradiation (without the addition of studied silicate powders) was used to eradicate pathogenic cells. As can be seen in Fig. S6 (ESI†), ten minutes of irradiation of pathogens resulted in a reduction in the number of viable cells forming a biofilm by $75 \pm 2\%$, $58 \pm 2\%$ and $70 \pm 2\%$ for *S. aureus*, *A. baumannii* and *C. albicans*, respectively. It should be noted, however, that the application of inorganic luminescent materials in anti-bacterial treatments offers several advantages when compared to standard antibiotic or UV light-based therapies. Such materials can be very effectively incorporated within the surfaces and fabrics, thus providing light activated decontamination, and, additionally, being inorganic ones, they provide prolonged chemical and optical stability (*i.e.* multiple anti-bacterial treatment rounds are possible with the use of the same material).

Conclusions

In summary, a series of doped yttrium silicate powders was synthesized to target biofilms formed by three different microorganisms (*S. aureus*, *A. baumannii*, and *C. albicans*) after Vis light irradiation. The materials were designed to produce up-conversion Vis-to-UV emission lines and by the careful selection of doping ions (Pr^{3+}, Tm^{3+}, and Yb^{3+}) we were able to obtain emission in UVC and UVA wavelength regions and further study their impact on the bacteria viability rates. In other words, we have shown yet another possibility to enhance the anti-microbial efficiency of the so-called benchmark material (*i.e.* yttrium silicates) for Pr^{3+} based Vis-to-UVC up-conversion. Additional co-doping with Tm^{3+} allowed the $Pr^{3+} \rightarrow Tm^{3+}$ energy transfer and the occurrence of an emission band in the UVA region. The combined effect of UVA and UVC emission generated *via* UC processes shows the potential for more effective photo-eradication of biofilms and is even more efficient for the planktonic cell destruction. It was also presented that the suspended microorganisms could be effectively killed by different Vis-to-UVA/UVC emission generated from $Y_2Si_2O_7$:Pr^{3+},Tm^{3+},Yb^{3+} phosphors and in some cases the

viability decreased down to $\sim 2\%$. Based on the obtained results, and comparison with the literature data, we believe that with further optimization to enhance emission lifetime and intensity, this system can potentially provide an alternative to achieve the required biocide activity. Thus, the continuous development of silicate phosphors and their derivatives with superior performance is a priority for future research efforts. A material capable of *ca.* 100 times greater Vis-to-UVC conversion efficiency would almost certainly make an up-conversion anti-microbial surface an effective and highly practical technology with considerable advantages over existing antimicrobial concepts. The lanthanide doped powders showing efficient Vis-to-UV UC emission could be used as doping materials in non-toxic polymers, for preventing direct contact between powders and *e.g.* skin, and lead to the preparation of modern optically activated in a site specific manner, self-sterilizing surfaces that could be applied in various areas of human life. Additionally, due to the potential site specify and on-demand laser light activated mode of action, the bio-safety concerns of using UV light should be sustained. One should realize that the widespread use of antibiotics and biocides leads to the development of cross-resistance of pathogens to these agents and the search for non-chemical methods of combating microorganisms is currently greatly increasing. Thus, we believe the presented luminescent powder-based solution towards disinfection purposes can be considered as an interesting alternative for already existing techniques, which, however, require further development.

Author contributions

P. F. – investigation, methodology, visualization, writing – original draft; M. Y. T. – investigation, methodology; I. M. – investigation, methodology; writing – original draft; S. J. Z. – investigation, methodology; B. C. – investigation, methodology; T. Y. O. – funding acquisition, writing – review & editing; M. S. – writing – review & editing; M. N. – conceptualization, writing – review & editing; D. W. – conceptualization, funding acquisition, supervision, visualization, writing – review & editing.

Conflicts of interest

There are no conflicts to declare.

Acknowledgements

References

1 M. T. Madigan, J. M. Martinko, P. V. Dunlap and D. P. C. Clark, *Brock Biology of Microorganisms*, Pearson Benjamin Cummings, San Francisco, CA, 12th edn, 2009.

2 S. McCarlie, C. E. Boucher and R. R. Bragg, *Drug Resist. Updates*, 2020, **48**, 100672.

3 A. Colclough, J. Corander, S. K. Sheppard, S. C. Bayliss and M. Vos, *Evol. Appl.*, 2019, **12**, 878–887.

4 World Health Organization, WHO global strategy for containment of antimicrobial resistance, 2001.

5 A. L. Santos, V. Oliveira, I. Baptista, I. Henriques, N. C. M. Gomes, A. Almeida, A. Correia and Â. Cunha, *Arch. Microbiol.*, 2013, **195**, 63–74.

6 M. Y. Tsang, P. Fałat, M. A. Antoniak, R. Ziniuk, S. J. Zelewski, M. Samoć, M. Nyk, J. Qu, T. Y. Ohulchanskyy and D. Wawrzyńczyk, *Nanoscale*, 2022, **39**, 14770–14778.

7 M. Ploydaeng, N. Rajatanavin and P. Rattanakaemakorn, *Photodermatol. Photoimmunol. Photomed.*, 2021, **37**, 12–19.

8 A. Rezaie, G. G. S. Leite, G. Y. Melmed, R. Mathur, M. J. Villanueva-Millan, G. Parodi, J. Sin, J. F. Germano, W. Morales, S. Weitsman, S. Y. Kim, J. H. Park, S. Sakhaie and M. Pimentel, *PLoS One*, 2020, **15**, 1–19.

9 E. Kvam and K. Benner, *J. Photochem. Photobiol., B*, 2020, **209**, 111899.

10 S. H. Livingston, J. L. Cadnum, K. J. Benner and C. J. Donskey, *Am. J. Infect. Control.*, 2020, **48**, 337–339.

11 E. G. Mbonimpa, E. R. Blatchley, B. Applegate and W. F. Harper, *J. Water Health*, 2018, **16**, 796–806.

12 A. Argyraki, M. Markvart, L. Bjørndal, T. Bjarnsholt and P. M. Petersen, *J. Biomed. Opt.*, 2017, **22**, 065004.

13 Y. Xiao, X. N. Chu, M. He, X. C. Liu and J. Y. Hu, *Water Res.*, 2018, **141**, 279–288.

14 K. Song, F. Taghipour and M. Mohseni, *Sci. Total Environ*, 2019, **665**, 1103–1110.

15 Y. Muramoto, M. Kimura and S. Nouda, *Semicond. Sci. Technol.*, 2014, **29**, 84004.

16 R. S. Bergman, *Photochem. Photobiol.*, 2021, **97**, 466–470.

17 Y. Du, X. Ai, Z. Li, T. Sun, Y. Huang, X. Zeng, X. Chen, F. Rao and F. Wang, *Adv. Photonics Res.*, 2021, **2**, 2000213.

18 Q. Su, H. L. Wei, Y. Liu, C. Chen, M. Guan, S. Wang, Y. Su, H. Wang, Z. Chen and D. Jin, *Nat. Commun.*, 2021, **12**, 4367.

19 D. Wawrzyńczyk, B. Cichy, J. K. Zaręba and U. Bazylińska, *J. Mater. Chem. C*, 2019, **7**, 15021–15034.

20 A. Gnach, K. Prorok, M. Misiak, B. Cichy and A. Bednarkiewicz, *J. Rare Earths*, 2014, **32**, 207–212.

21 A. Zhang, Z. Sun, M. Jia, G. Liu, F. Lin and Z. Fu, *J. Chem. Eng.*, 2019, **365**, 400–404.

22 J. Wu, H. Zheng, X. Liu, B. Han, J. Wei and Y. Yang, *Opt. Lett.*, 2016, **41**, 792–795.

23 X. Zhao, F. Liu, T. Shi, H. Wu, L. Zhang, J. Zhang, X. Wang and Y. Liu, *Adv. Photonics Res.*, 2022, **3**, 2200106.

24 P. Lv, L. Li, Z. Yin, C. Wang and Y. Yang, *Opt. Lett.*, 2022, **47**, 4435–4438.

25 C. Cao, W. Qin, J. Zhang, Y. Wang, P. Zhu, G. Wei, G. Wang, R. Kim and L. Wang, *Opt. Lett.*, 2008, **33**, 857–859.

26 E. L. Cates, M. Cho and J. H. Kim, *Environ. Sci. Technol.*, 2011, **45**, 3680–3686.

27 E. L. Cates and F. Li, *RSC Adv.*, 2016, **6**, 22791–22796.

28 D. G. J. Larsson and C. F. Flach, *Nat. Rev. Microbiol.*, 2022, **20**, 257–269.

29 U. Kumar, C. R. Fox, E. Kolanthai, C. J. Neal, K. Kedarinath, Y. Fu, E. Marcelo, B. Babu, G. D. Parks and S. Seal, *ACS Appl. Mater. Interfaces*, 2022, **14**, 40659–40673.

30 C. Wang, L. Li, P. Lv, L. Zi, S. Feng, F. Yang, J. Qiu and Y. Yang, *J. Mater. Chem. C*, 2023, **11**, 8495–8501.

31 H. Zhao, L. Zhang, J. Lu, S. Chai, J. Wei, Y. Yu, R. Miao and L. Zhong, *J. Mater. Chem. B*, 2023, **11**, 2745–2753.

32 E. Grela, J. Kozłowska and A. Grabowiecka, *Acta Histochem.*, 2018, **120**, 303–311.

33 L. Sun, C. Qian, C. Liao, X. Wang and C. Yan, *Solid State Commun.*, 2001, **119**, 393–396.

34 A. I. Becerro and A. Escudero, *Chem. Mater.*, 2005, **17**, 112–117.

35 E. L. Cates, A. P. Wilkinson and J. H. Kim, *J. Phys. Chem. C*, 2012, **116**, 12772–12778.

36 M. E. Fleet and X. Liu, *Z. Kristallogr.-Cryst. Mater.*, 2003, **218**, 795–801.

37 M. E. Fleet and X. Liu, *Acta Crystallogr. B*, 2000, **56**, 940–946.

38 X. Xu, Z. Xiao, Y. Wang, Y. Yan, J. Shen, Y. Nie, W. You, D. Wu, L. Han and F. Lai, *Opt. Mater.*, 2022, **134A**, 113191.

39 F. Reichert, F. Moglia, M. Fechner, N. O. Hansen, D. T. Marzahl and G. Huber, *Opt. Express*, 2012, **20**, 20387–20395.

40 C. Li, A. Lagriffoul, R. Moncorge, J. C. Souriau, C. Borel and C. Wyon, *J. Lumin.*, 1994, **62**, 157–171.

41 X. Wang, J. Qiu, J. Song, J. Xu, Y. Liao, H. Sun, Y. Cheng and Z. Xu, *Opt. Commun.*, 2008, **281**, 299–302.

42 S. Heer, K. Kömpe, H. U. Güdel and M. Haase, *Adv. Mater.*, 2004, **16**, 2102–2105.

43 A. Kumari and V. K. Rai, *AIP Conf. Proc.*, 2015, **1661**, 100006.

44 C. Hu, C. Sun, J. Li, Z. Li, H. Zhang and Z. Jiang, *Chem. Phys.*, 2006, **325**, 563–566.

45 J. D. Hoerter, A. A. Arnold, D. A. Kuczynska, A. Shibuya, C. S. Ward, M. G. Sauer, A. Gizachew, T. M. Hotchkiss, T. J. Fleming and S. Johnson, *J. Photochem. Photobiol., B*, 2005, **81**, 171–180.

46 N. Zhao, L. P. Lv, P. Ma, Y. Y. Zhang, J. Deng and Y. Y. Zhang, *J. Photochem. Photobiol., B*, 2023, **239**, 112641.

47 R. M. Donlan and J. W. Costerton, *Clin. Microbiol. Rev.*, 2002, **15**, 167–193.

48 H. Wu, C. Moser, H. Z. Wang, N. Høiby and Z. J. Song, *Int. J. Oral Sci.*, 2015, **7**, 1–7.

49 R. Roy, M. Tiwari, G. Donelli and V. Tiwari, *Virulence*, 2018, **9**, 522–554.

50 H. van Acker, P. van Dijck and T. Coenye, *Trends Microbiol.*, 2014, **22**, 326–333.

51 I. Mitra, S. Mukherjee, P. B. Reddy Venkata, S. Dasgupta, C. K. Jagadeesh Bose, S. Mukherjee, W. Linert and S. C. Moi, *RSC Adv.*, 2016, **6**, 76600–76613.

52 A. Karami, F. Farivar, T. J. De Prinse, H. Rabiee, S. Kidd, C. J. Sumby and J. Bi, *ACS Appl. Bio Mater.*, 2021, **4**, 6125–6136.

53 M. Tou, Z. Luo, S. Bai, F. Liu, Q. Chai, S. Li and Z. Li, *Mater. Sci. Eng., C*, 2017, **70**, 1141–1148.

54 Y. Zhang, P. Huang, D. Wang, J. Chen, W. Liu, P. Hu, M. Huang, X. Chen and Z. Chen, *Nanoscale*, 2018, **10**, 15485–15495.

55 W. Liu, Y. Zhang, W. You, J. Su, S. Yu, T. Dai, Y. Huang, X. Chen, X. Song and Z. Chen, *Nanoscale*, 2020, **12**, 13948–13958.

56 A. Karami, H. Zhang, V. G. Pederick, C. A. McDevitt, M. S. Kabir, S. Xu, P. Munroe, Z. Zhou and Z. Xie, *Surf. Eng.*, 2019, **35**, 596–603.

57 N. Hadrup, A. K. Sharma and K. Loeschner, *Regul. Toxicol. Pharmacol.*, 2018, **98**, 257–267.